RESEARCH ARTICLE

An F876L Mutation in Androgen Receptor Confers Genetic and Phenotypic Resistance to MDV3100 (Enzalutamide)

Manav Korpal[1], Joshua M. Korn[1], Xueliang Gao[3], Daniel P. Rakiec[2], David A. Ruddy[2], Shivang Doshi[1], Jing Yuan[1], Steve G. Kovats[1], Sunkyu Kim[1], Vesselina G. Cooke[1], John E. Monahan[2], Frank Stegmeier[1], Thomas M. Roberts[3], William R. Sellers[1], Wenlai Zhou[1], and Ping Zhu[1]

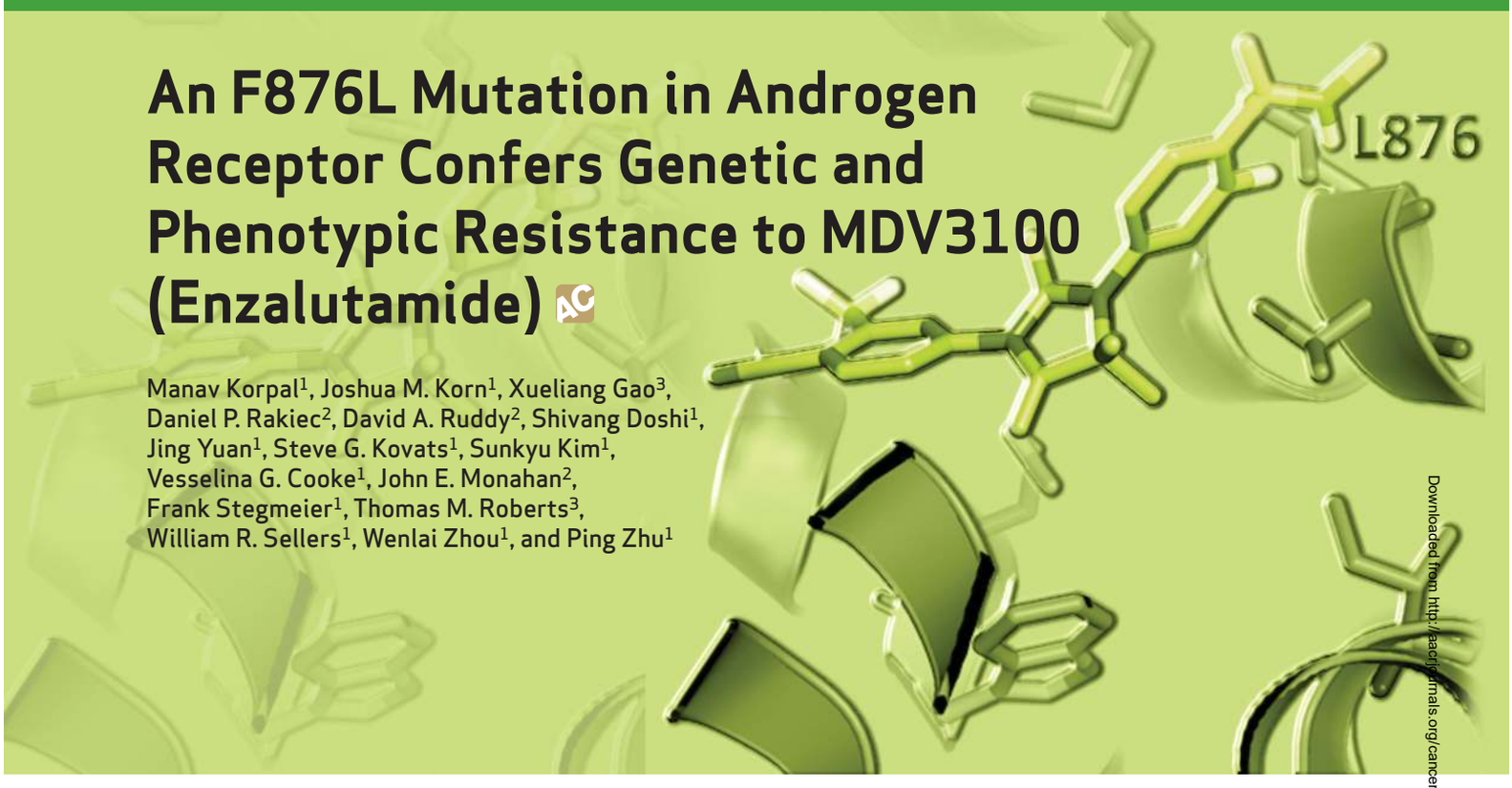

ABSTRACT

Castration-resistant prostate cancer (CRPC) is the most aggressive, incurable form of prostate cancer. MDV3100 (enzalutamide), an antagonist of the androgen receptor (AR), was approved for clinical use in men with metastatic CRPC. Although this compound showed clinical efficacy, many initial responders later developed resistance. To uncover relevant resistant mechanisms, we developed a model of spontaneous resistance to MDV3100 in LNCaP prostate cancer cells. Detailed characterization revealed that emergence of an F876L mutation in AR correlated with blunted AR response to MDV3100 and sustained proliferation during treatment. Functional studies confirmed that AR^{F876L} confers an antagonist-to-agonist switch that drives phenotypic resistance. Finally, treatment with distinct antiandrogens or cyclin-dependent kinase (CDK)4/6 inhibitors effectively antagonized AR^{F876L} function. Together, these findings suggest that emergence of F876L may (i) serve as a novel biomarker for prediction of drug sensitivity, (ii) predict a "withdrawal" response to MDV3100, and (iii) be suitably targeted with other antiandrogens or CDK4/6 inhibitors.

SIGNIFICANCE: We uncovered an F876L agonist-switch mutation in AR that confers genetic and phenotypic resistance to the antiandrogen drug MDV3100. On the basis of this finding, we propose new therapeutic strategies to treat patients with prostate cancer presenting with this AR mutation. *Cancer Discov; 3(9); 1030–43. ©2013 AACR.*

See related commentary by Nelson and Yegnasubramanian, p. 971.

Authors' Affiliations: [1]Oncology Disease Area, [2]Department of Oncology Translational Medicine, Novartis Institutes for BioMedical Research, Cambridge; and [3]Department of Cancer Biology, Dana-Farber Cancer Institute, Harvard Medical School, Boston, Massachusetts

Note: Supplementary data for this article are available at Cancer Discovery Online (http://cancerdiscovery.aacrjournals.org/).

J.M. Korn and X. Gao contributed equally to this work.

Current affiliation for P. Zhu: Department of Target Discovery & Genomics, H3 Biomedicine, Cambridge, Massachusetts.

Corresponding Authors: Manav Korpal, Oncology Disease Area, Novartis Institutes for BioMedical Research, 250 Massachusetts Avenue, Cambridge, MA 02139. Phone: 857-210-2139; E-mail: manav.korpal@outlook.com; and William R. Sellers, William.Sellers@novartis.com

doi: 10.1158/2159-8290.CD-13-0142

INTRODUCTION

Prostate cancer is one of the most commonly diagnosed cancers among men worldwide (1, 2). Although localized tumors are often successfully treated, distant metastases emerge in a significant fraction of patients (3, 4). Androgen-deprivation therapy is initially effective; however, almost invariably resistance emerges and results in a much more aggressive form of tumor referred to as castration-resistant prostate cancer (CRPC). CRPC is the second most common cause of cancer-related death in American men (5) and is currently incurable. A conserved feature of CRPC is the sustained activity of androgen receptor (AR)-signaling (6), by virtue of mechanisms including *AR* gene overexpression/amplification and *AR* gene mutations (3). These data have suggested that prostate cancer may largely remain dependent on AR signaling.

The continued reliance on AR signaling in CRPC has led to the development of CYP17 inhibitors (abiraterone) and improved antagonists that compete with androgens for binding to the ligand-binding pocket of AR. MDV3100 (enzalutamide) is a novel antiandrogen that was recently approved by the U.S. Food and Drug Administration for treatment of men with metastatic CRPC previously treated with docetaxel. Although MDV3100 has shown significant efficacy in clinical trials, many patients who initially responded favorably develop resistance to this second-generation antiandrogen (7). The molecular mechanisms driving resistance, however, are currently unclear, and a deeper understanding is critical for the rational development of alternate therapeutics.

In vitro and *in vivo* experimental models of resistance serve as useful tools for expeditious discovery of mechanisms that allow drug escape, and for the evaluation of alternate therapies. We here present the derivation of a model of spontaneous resistance in LNCaP cells, which led to the identification of a novel F876L mutation in *AR* that potently drives genetic/phenotypic resistance to MDV3100. This mutation allows AR-F876L to use MDV3100 as an agonist and ultimately promotes an addiction phenotype *in vivo*. These data continue to support the notion that despite improved AR antagonists, prostate cancer cells remain dependent on AR signaling, and hence evolve specific mutations to overcome antiandrogen therapies. Because we further show that the F876L variant retains sensitivity to bicalutamide, combination therapy with structurally distinct antiandrogens either in parallel or in series together with androgen deprivation may provide an appealing therapeutic strategy for combating AR-mediated resistance mechanisms in the clinic. Furthermore, in addition to targeting the hypermutable AR ligand-binding domain, we show that targeting downstream or interactive effectors of AR signaling, such as cyclin-dependent kinases (CDK)4/6, provides an alternative strategy for overcoming resistance mechanisms when AR-directed therapies become ineffective.

RESULTS

Development and Characterization of a Model of Spontaneous Resistance to MDV3100

To facilitate the discovery of resistance mechanisms, we generated a model of spontaneous resistance in LNCaP cells. Although short-term culture of LNCaP cells with MDV3100 (<1.5 months) induced population-wide stasis [Fig. 1A, fetal calf serum (FCS) + MDV3100 relative to FCS], long-term culture with 1 μmol/L MDV3100 led to the emergence of resistant clones (Fig. 1B). After isolation and expansion, resistant clones that displayed similar growth properties as the control populations (C1–C3; Fig. 1B) were chosen for further characterization. Short-term (Fig. 1C) and long-term (Supplementary Fig. S1) proliferation assays confirmed the resistance phenotype. Specifically, four of seven resistant clones (#1, 15, 19, and 24; strongly resistant, green curves and font) displayed significantly higher resistance to MDV3100 than weakly resistant clones (#9, 10, and 14; red curves and font) or the control lines (C1–C3; brown curves and font; Fig. 1C). In contrast, strongly resistant clones displayed sensitivity to bicalutamide (Fig. 1C), cumulatively suggesting that the mechanism(s) of resistance in strongly resistant clones may be fine-tuned to specifically promote resistance to MDV3100.

To elucidate mechanism(s) of resistance, we first analyzed expression levels of AR, as its overexpression has previously been shown to promote resistance to castrate levels of androgens (6) and the antiandrogen bicalutamide (1). Here, we did not observe a significant change in AR expression (Fig. 1D), and global gene expression analysis of AR pathway activity showed a lack of significant modulation of the AR pathway at baseline (Fig. 1E, beige bars).

Strongly Resistant Clones Show Blunted AR Pathway Response to MDV3100

To further explore the molecular mechanisms that drive resistance, we conducted gene-expression microarray analysis on RNA derived from three controls and seven resistant clones treated with dimethyl sulfoxide (DMSO) or MDV3100 for 24 hours. Unbiased hierarchical clustering of the transcriptional effects in response to MDV3100 treatment revealed that the strongly resistant clones clearly segregated from the weakly resistant and control lines (Fig. 2A, left), supporting the phenotypic differences described earlier (Fig. 1C). Further interrogation of the data revealed four distinct gene expression patterns (labeled I–IV). Although pathway enrichment analysis (8) failed to reveal a significant enrichment of pathway signatures in classes I, II, and IV, a strong enrichment of genes involved in AR pathway activation was observed in class III (Fig. 2A, middle and right, and Supplementary Table S1). These data suggested that strongly resistant cell lines could at least maintain AR pathway activity despite continuous exposure to MDV3100. In keeping with this notion, clustering (Supplementary Fig. S2A), pathway enrichment analysis (Fig. 2B and Supplementary Fig. S2B), and quantitative PCR (qPCR) analysis of three AR target genes (Fig. 2C) confirmed that MDV3100 treatment downregulated AR pathway activity in control and weakly resistant lines but not in the strongly resistant clones.

The mechanism by which MDV3100 inhibits AR signaling has been attributed partially to its ability to hinder nuclear translocation of AR (9). We therefore determined whether localization of AR was altered in the resistant clones in

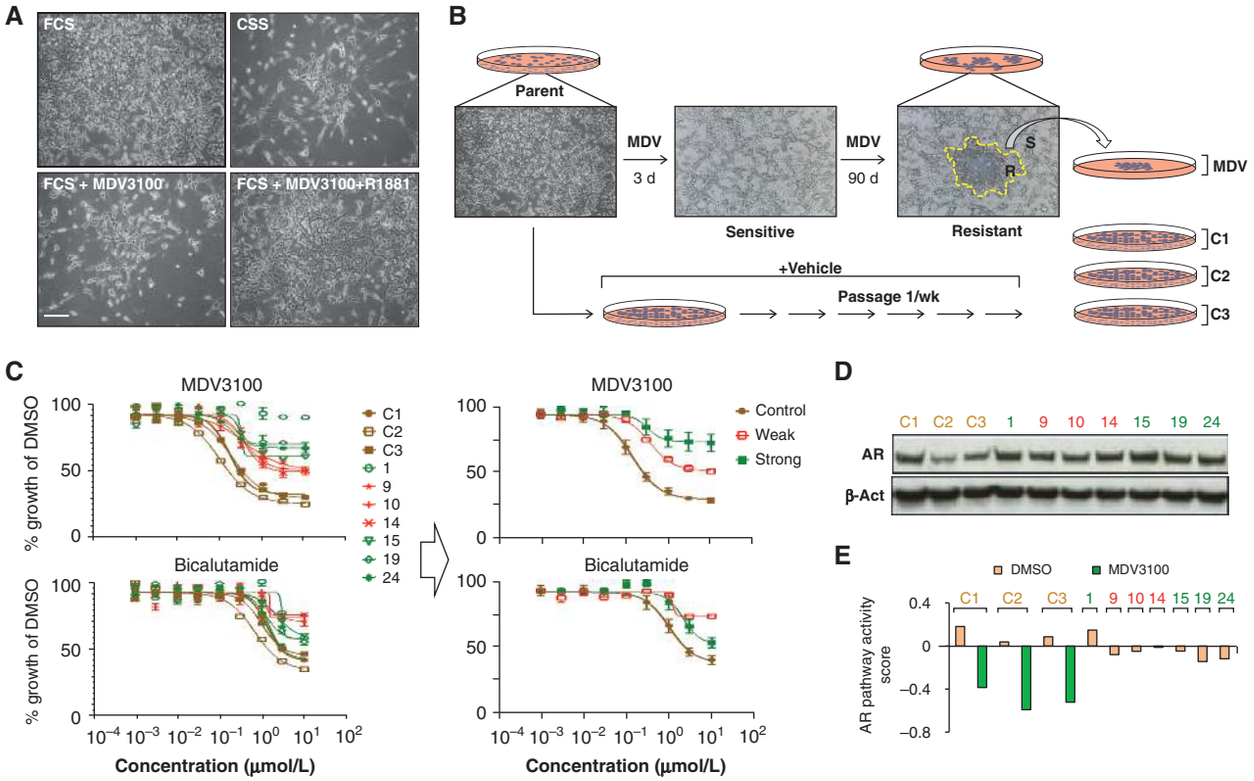

Figure 1. Characterization of MDV3100-resistant clones derived from LNCaP cells. **A,** phase contrast images of LNCaP cells grown in RPMI media supplemented with 10% FCS (top left), 10% CSS (top right), 10% FCS + 1 μmol/L MDV3100 (bottom left), and 10% FCS + 1 μmol/L MDV3100 + 1 nmol/L R1881 (bottom right). Scale bar, 50 μm. **B,** schematic representation of the experimental paradigm applied (see main text for details). **C,** individual (left) and average (right) growth inhibition curves for the three controls (brown line) and seven resistant clones (green and red) treated with MDV3100 (top) and bicalutamide (bottom). Data presented as percentage of growth relative to DMSO treatment condition as measured by CellTiter-Glo assay. **D,** Western blot analysis of AR expression in control and resistant lines. β-Actin (β-Act) used as loading control. **E,** AR pathway activity scores for C1–C3 and seven resistant clones grown in 10% FCS at baseline (following drug withdrawal for 2 weeks; beige bars). Scores also calculated for C1–C3 treated with 10 μmol/L MDV3100 for 24 hours as reference (green bars). Genes upregulated by androgens were used for analysis.

response to MDV3100. To this end, cytoplasmic and nuclear protein fractions from a control (C1) and strongly resistant (clone #1) line treated with DMSO or MDV3100 were isolated. In contrast to C1, where MDV3100 significantly reduced nuclear AR localization (nuclear:cytoplasmic ratio: DMSO = 0.46, MDV = 0.07), MDV3100 treatment did not significantly alter AR nuclear localization in the strongly resistant clone (nuclear:cytoplasmic ratio: DMSO = 0.59, MDV = 0.49; Fig. 2D and Supplementary Fig. S3), supporting the notion that AR remains activated in the strongly resistant cell lines.

Whole-Transcriptome Sequencing Uncovers a Novel *AR* Mutation Correlated with Resistance

To define the mechanism(s) underlying resistance to MDV3100, we next conducted whole-transcriptome sequencing on nine of 10 lines described above. Expressed protein-coding sequence variants were identified and compared with sequences in parental control lines. Somatic mutations found in more than one clone, but with discordant genotypes across clones, were used to cluster the samples using hierarchical clustering (Fig. 3A). Although there were many recurrent mutations, only one candidate, a recurrent F876L mutation in the *AR* gene, was conserved among all four strongly resistant clones and not found in weakly resistant or control lines (Fig. 3A and Supplementary Table S2). Interestingly, clone #19 presented a very distinct mutational spectrum compared with other strongly resistant clones, likely suggesting that AR^{F876L} occurred by independent mechanisms in these subclones (Fig. 3A).

The F876L mutation is localized to the ligand-binding domain of AR and is adjacent to the homozygous T877A mutation in LNCaP cells (Fig. 3B), a mutation previously shown to confer resistance to hydroxyflutamide (10–12). In all cases, the mutation was heterozygous with a mutant allelic mRNA frequency of approximately 40%, with the exception of clone #15, which presented the lowest frequency at 20% (Fig. 3B, right). The presence of the F876L mutation in genomic DNA was confirmed by Sanger sequencing (Supplementary Fig. S4).

Having shown that AR^{F876L} spontaneously emerges in a majority of the MDV3100-resistant clones, we next aimed to assess whether AR^{F876L} is also detectable in MDV3100-resistant tumors using an *in vivo* xenograft model (Fig. 3C). Strikingly, whole-transcriptome sequencing revealed that three of four resistant tumors harbored the F876L mutation (Fig. 3D), with frequencies ranging from 46% to 52% of the total *AR* transcript reads (Fig. 3E). Interestingly, there were two unique nucleotide substitutions observed promoting

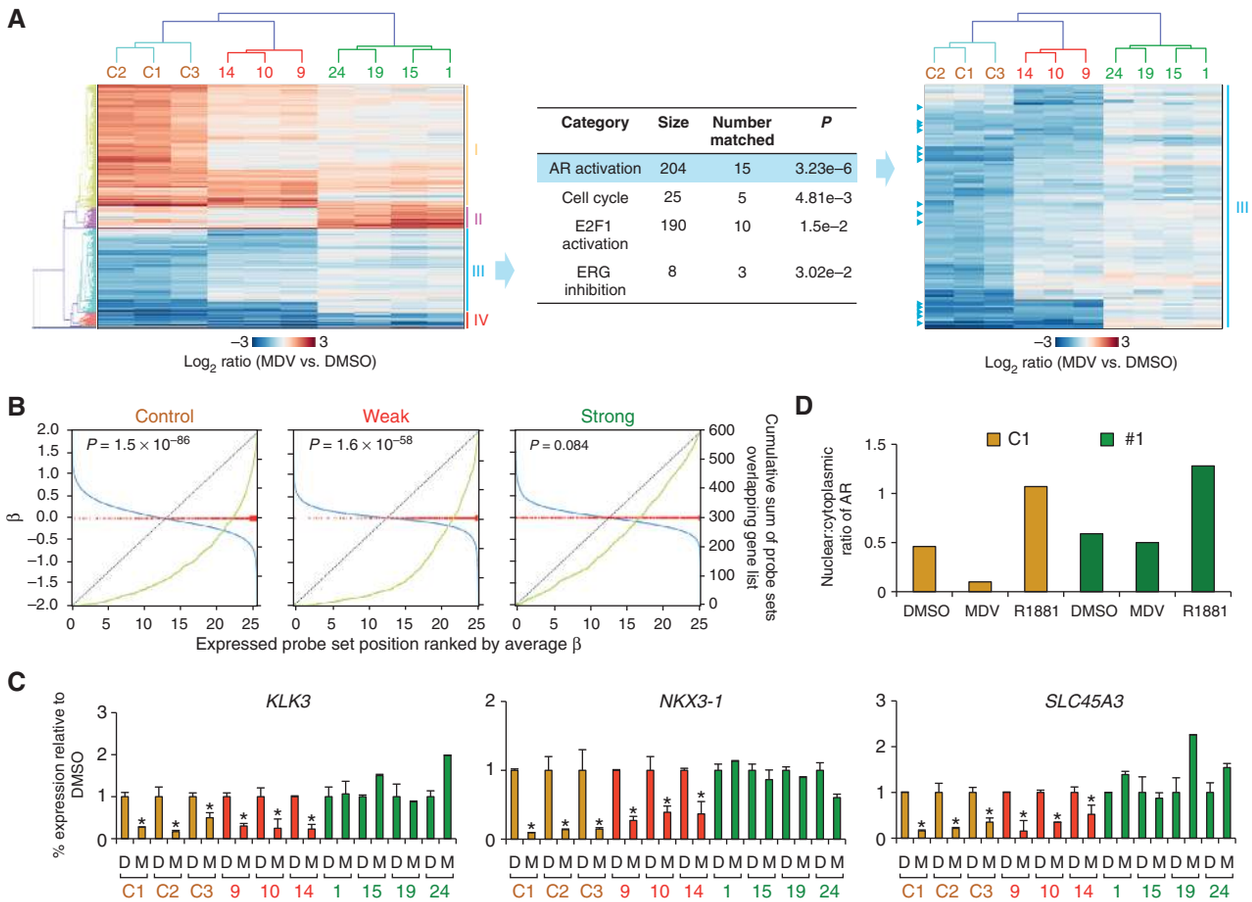

Figure 2. Resistant clones segregate based on AR pathway sensitivity to MDV3100. **A,** left, heatmap showing differential expression of genes in control (brown font), weakly resistant lines (red), and strongly resistant lines (green) upon treatment with 10 μmol/L MDV3100 for 24 hours. Probe sets with an average fold change of at least 2 (MDV vs. DMSO) for at least one sample set (controls, weakly resistant samples, and strongly resistant samples) are shown. Roman numerals listed on right represent broad classes of differentially expressed genes. Middle, table showing results from GO pathway enrichment analysis of genes from class III. Blue shade highlights significant enrichment of genes from the "AR activation" gene set. Right, zoomed image of class III showing relative location of AR-regulated genes (blue arrowheads) that add to significance score from pathway analysis. All data presented as $\log_2$ ratio of MDV versus DMSO treatment. **B,** correlation between an AR gene signature in comparison with the top-ranked genes upon treatment with 10 μmol/L MDV3100 for 24 hours in controls (left), weakly resistant lines (middle), and strongly resistant lines (right). Green line represents level of pathway activity—stronger deviation from black diagonal represents greater inhibition of pathway activity by MDV3100 treatment. **C,** qPCR analysis of expression of canonical AR target genes in 10 lines treated with DMSO or MDV3100 for 24 hours. Data are presented as percentage of expression in MDV3100-treated sample relative to DMSO (arbitrarily set at 100%). **D,** DMSO; M, 10 μmol/L MDV3100. *TBP* was used to normalize expression. Data represent mean ± SEM; $n = 3$. *, $P < 0.05$ (Student *t* test). **D,** quantitation of nuclear to cytoplasmic ratio of endogenous AR expression in control (C1, brown) and resistant clone (#1, green) treated with DMSO, 10 μmol/L MDV3100 (MDV), or 0.1 nmol/L R1881 (R1881) for 24 hours. Western blot analysis data presented in Supplementary Fig. S3 was analyzed by ImageJ to determine ratios.

F876L, implying that these mutations may have been acquired during the course of treatment (Fig. 3D and E). Furthermore, the MDV3100-resistant tumor lacking AR^{F876L} showed the slowest growth kinetics in the presence of MDV3100 (Fig. 3C), and lowest expression of AR target genes *KLK3* and *NKX3-1* relative to those harboring the mutation (Fig. 3F). Cumulatively, these data strongly suggest that emergence of AR^{F876L} may represent a dominant tumor-autonomous mechanism of resistance to MDV3100.

AR^{F876L} Confers an Antagonist-to-Agonist Switch for MDV3100

To assess the potential impact of the F876L mutation on MDV3100 response, we computationally modeled the binding of MDV3100 to the wild-type (WT) and mutant receptors. We found that in the docking modes of the antagonistic state of WT AR, MDV3100 displayed only a weak interaction with F876 (Fig. 4A, left). However, in the presence of the F876L mutation, the benzamide motif of MDV3100 can extend into the access channel created by the smaller leucine residue. This would potentially prevent the compound from clashing with helix-12 of the AR ligand-binding domain in the agonistic mode (Fig. 4A, right). Thus, computational modeling suggested that F876L mutation in AR may abolish the antagonistic activity of MDV3100 and could potentially allow agonist activity.

To functionally test the impact of the F876L mutation, we next assessed the transcriptional responses of the WT

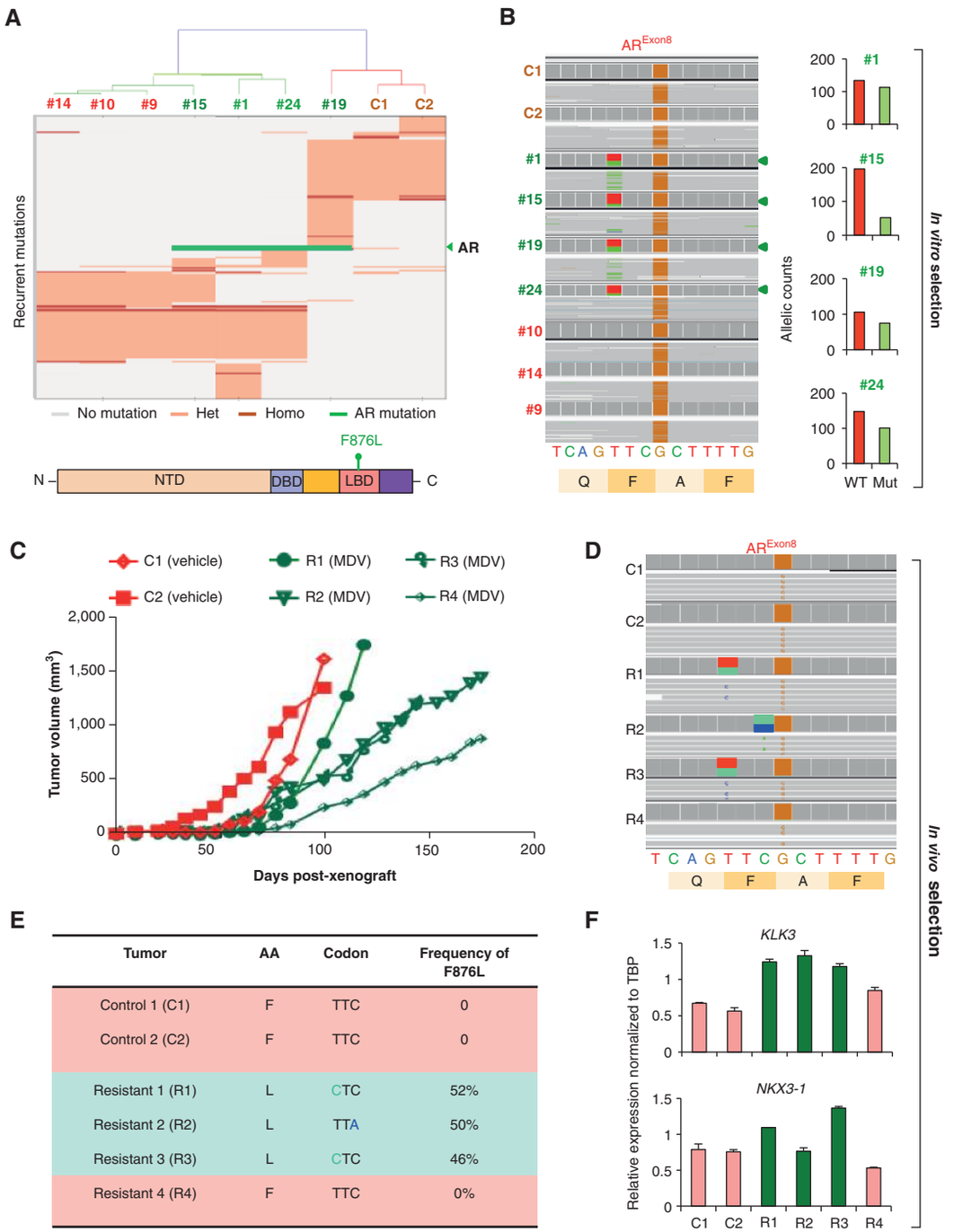

Tumor	AA	Codon	Frequency of F876L
Control 1 (C1)	F	TTC	0
Control 2 (C2)	F	TTC	0
Resistant 1 (R1)	L	CTC	52%
Resistant 2 (R2)	L	TTA	50%
Resistant 3 (R3)	L	CTC	46%
Resistant 4 (R4)	F	TTC	0%

Figure 3. Whole-transcriptome sequencing analysis identifies a novel F876L mutation in *AR* in strongly resistant lines and xenograft tumors. **A,** top, unbiased hierarchical clustering of somatic mutations detected in controls (brown font), weakly resistant clones (red font), and strongly resistant clones (green font). Gray line represents lack of mutation; orange line represents single recurrent heterozygous mutation; red line represents recurrent homozygous mutation; green line represents recurrent mutation in AR, as indicated by green arrowhead. Bottom, schematic of human AR. NTD, N-terminal domain; DBD, DNA-binding domain; LBD, ligand-binding domain. Site of F876L mutation indicated by green line and green font. **B,** left, IGV plot showing heterozygous nature of F876L mutation in exon 8 of *AR* in strongly resistant clones (indicated by green arrowheads). F876L mutation is adjacent to a preexisting homozygous T877A mutation (orange shade) in LNCaP. Right, raw counts of WT (red shade) and mutant (Mut, green shade) *AR* alleles in strongly resistant clones. **C,** tumor growth kinetics of two vehicle-treated (red curves) and four MDV3100-treated (green curves) LNCaP tumors. **D,** IGV plot showing the relative position and frequency of nucleotide substitutions promoting F876L in MDV3100-resistant tumors. C1–C2, vehicle-treated tumors; R1–R4, MDV3100-resistant tumors. **E,** table summarizing data from IGV plot. Red shade represents tumors bearing WT *AR*, whereas green shade highlights tumors bearing F876L-mutant *AR*. **F,** bar graphs showing relative expression of AR target genes *KLK3* and *NKX3-1* in LNCaP tumors. Red bars, expression data from tumors expressing AR-WT; green bars, expression data from tumors harboring AR^{F876L}. IGV, Integrative Genomics Viewer.

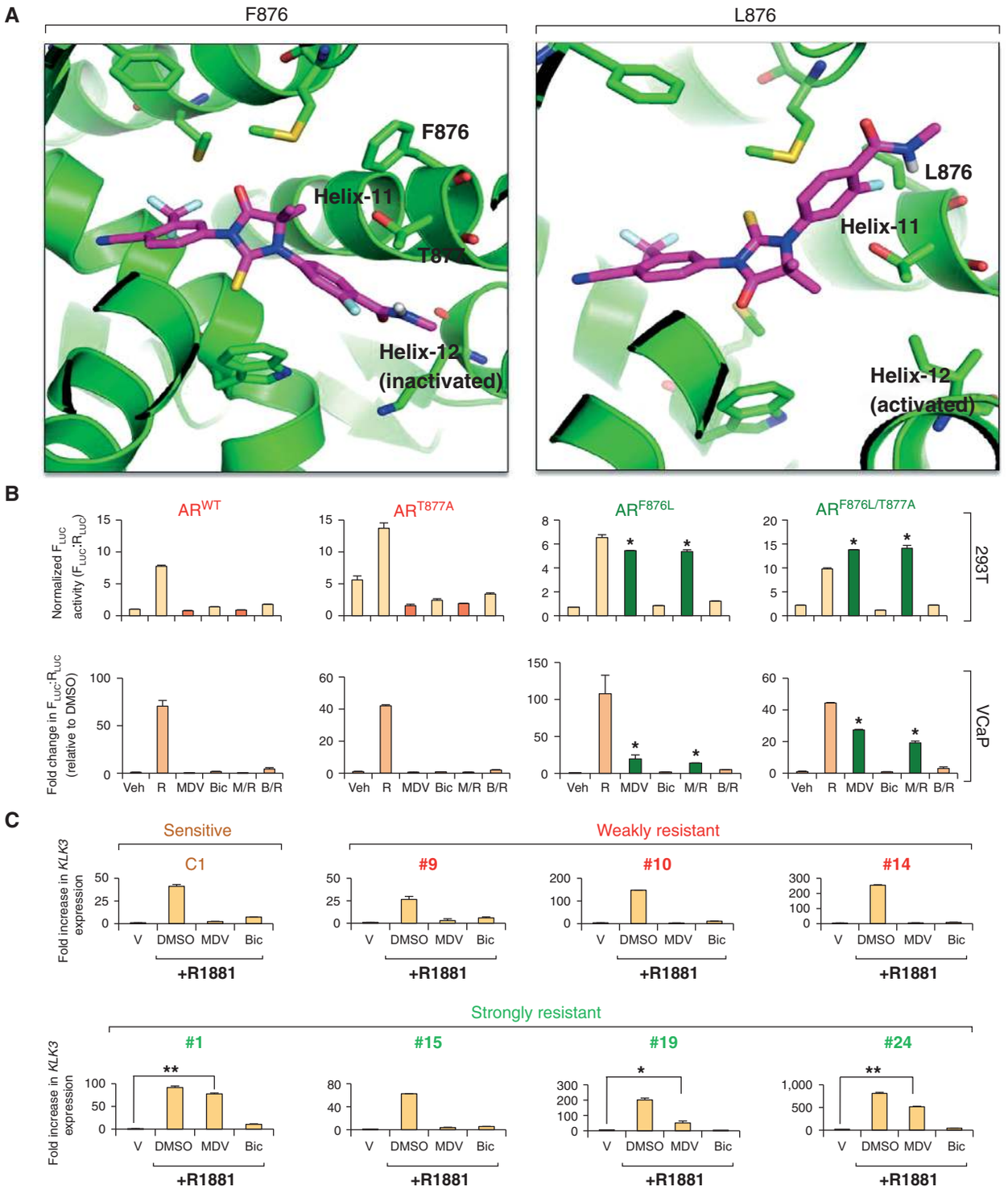

Figure 4. F876L mutation functionally confers an antagonist-to-agonist switch. **A,** comparison of the docking modes of MDV3100 in an inactivated state of WT AR (left) with a speculative model of MDV3100 bound to an activated state of mutant AR (right). **B,** bar graphs showing normalized AR reporter activity following transfection of 293T (top) and VCaP (bottom) cells with various AR expression constructs (AR^{WT}, AR^{T877A}, AR^{F876L}, and $AR^{F876L/T877A}$) and subsequent treatment with vehicle (Veh), 0.1 nmol/L R1881 (R), 10 μmol/L MDV3100 (MDV), 10 μmol/L bicalutamide (Bic), 10 μmol/L MDV3100 + 0.1 nmol/L R1881 (M/R), or 10 μmol/L bicalutamide + 0.1 nmol/L R1881 (B/R) for 24 hours. All data are normalized to *Renilla* luciferase (R_{LUC}) expression. Data represent mean ± SEM; $n = 3$. *, $P < 0.001$ (Student *t* test). **C,** qPCR analysis of *KLK3* expression in a control line (C1), weakly resistant clones (red font), and strongly resistant clones (green font) following treatment with vehicle (V), 0.1 nmol/L R1881, 0.1 nmol/L R1881 + 10 μmol/L MDV3100 (MDV), and 0.1 nmol/L R1881 + 10 μmol/L bicalutamide (Bic) in 10% CSS for 24 hours. *TBP* used to normalize expression. Data represent mean ± SEM; $n = 3$. *, $P < 0.05$; **, $P < 0.01$ (Student *t* test).

AR, single mutants T877A, W741C, W741L, and F876L, and the double mutant F876L/T877A to the agonistic synthetic androgen R1881 and the antiandrogens bicalutamide and MDV3100 in transactivation reporter assays using HEK293T cells. The W741C/L mutant has previously been shown to confer an agonist switch specific for bicalutamide and was used as a control (13). Notably, we found that only AR^{F876L} and $AR^{F876L/T877A}$ had a substantial transactivation response of an androgen response element (ARE)-driven reporter gene (14) to MDV3100—comparable with 0.1 nmol/L R1881—suggesting an antagonist-to-agonist switch exquisitely specific for MDV3100 (Fig. 4B and Supplementary Fig. S5A and S5B). These findings were further validated in AR^- PC3 (Supplementary Fig. S6) and AR^+ VCaP prostate cancer lines (Fig. 4B).

In support of the transactivation data, a similar agonist switch was also observed in spontaneously resistant clones that harbored the F876L mutation when *KLK3* expression was analyzed in response to MDV3100 in media stripped of endogenous androgens—a condition that minimized basal AR pathway activity and the response of endogenous WT AR to MDV3100 (Fig. 4C). Notably, although the most strongly resistant clones (#1, 19, and 24) expressed significantly higher levels of *KLK3* in the presence of MDV3100 relative to vehicle, clone #15 showed similar sensitivity to MDV3100 as the control (C1) and weakly resistant clones, likely attributable to the low mutant allelic mRNA frequency (Fig. 3B, right). These data in aggregate strongly suggest that the F876L mutation in AR is a driver of an antagonist-to-agonist switch highly specific for MDV3100.

The F876L Mutation Is Sufficient to Induce Genetic and Phenotypic Resistance to MDV3100 in Genetically Engineered LNCaP Cells

Given that strongly resistant clones harbor several sequence variants in addition to the F876L mutation, we wanted to formally test whether the AR^{F876L} variant is sufficient to promote an MDV3100-resistant growth phenotype. To this end, LNCaP cells were engineered to inducibly express the T877A-, F876L/T877A-, and W741C/T877A mutants (Supplementary Fig. S7). In support of previous reports, expression of all T877A-bearing mutant alleles and the W741C/T877A allele promoted an antagonist-to-agonist switch specific for hydroxyflutamide (10–12) and bicalutamide (13), respectively, based on the regulation of the AR target gene *KLK3* (*PSA*; Supplementary Fig. S8). Despite the slightly lower expression of $AR^{F876L/T877A}$, a significant rescue of AR pathway activity was observed under 10% FCS culture conditions (Fig. 5A and Supplementary Fig. S8), and a significant agonist effect was observed under 10% charcoal-stripped FCS (CSS) culture conditions (Supplementary Fig. S9A). The influence of $AR^{F876L/T877A}$ on pathway activity closely paralleled changes in localization of AR as $AR^{F876L/T877A}$ showed greater nuclear influx (MDV3100 vs. DMSO) relative to the T877A line, under both 10% FCS (Supplementary Fig. S10A and S10B) and 10% CSS (Fig. 5B, Supplementary Figs. S9B and S10B) culture conditions. Unexpectedly, we also observed a significant rescue of pathway activity in the W741C/T877A line, likely due to the constitutive active function conferred by the double mutation as reported previously (ref. 13; Fig. 5A and B).

Having established that $AR^{F876L/T877A}$ can use MDV3100 as an agonist, we next tested whether ectopic expression of $AR^{F876L/T877A}$ was sufficient to confer phenotypic resistance. Although only a modest rescue in growth was observed in a short-term proliferation assay (Supplementary Fig. S11A and S11B), a robust rescue was observed in a long-term colony formation assay in response to MDV3100, but not bicalutamide (Fig. 5C). Notably, the W741C/T877A line also showed significant growth in the presence of MDV3100 (Fig. 5C), consistent with the rescue of pathway activity observed earlier (Fig. 5A and B).

To assess whether the T877A mutation is necessary for the resistance phenotype, LNCaP cells were engineered to stably express the single-mutant AR^{F876L}. Consistent with the transactivation data (Fig. 4B and Supplementary Fig. S6), AR^{F876L} conferred genetic and phenotypic resistance to MDV3100, suggesting that F876L—alone or in conjunction with T877A—is equally capable of conferring an agonist switch (Supplementary Fig. S12A and S12B).

The Resistance-Conferring Role of AR^{F876L} Is Broadly Applicable to Several Prostate Cancer Lines

Given that the F876L mutation in AR can promote resistance to MDV3100 in *PTEN*-null LNCaP cells, we next questioned whether this mutation is sufficient to broadly confer resistance in prostate cancer lines of various genetic backgrounds. To this end, human VCaP (harboring *TMPRSS2–ERG* fusion and *AR* amplification) and murine Myc–CaP (overexpressing Myc) lines were transduced to stably express the mutant *AR*. Consistent with the resistance phenotype observed in LNCaP cells, both lines also presented partial resistance to MDV3100 (Fig. 5D and Supplementary Fig. S13), suggesting that F876L mutation in AR has the potential for conferring resistance to MDV3100 under various genetic contexts.

Taken together, our data implicate a direct role for AR-F876L, $AR^{F876L/T877A}$, and potentially constitutively active AR variants, such as W741C/T877A, as drivers of resistance to MDV3100. Although constitutively active variants may promiscuously promote resistance to various classes of antiandrogens, we show that F876L mutation in *AR* selectively promotes resistance to MDV3100.

AR^{F876L}-Bearing Cells Are Resistant to MDV3100 in the Castrate Setting *In Vivo*

Having shown that the F876L mutation in *AR* confers an agonist switch for MDV3100 that can promote resistance, we next asked whether F876L-bearing cells become dependent on this switch for cellular growth under androgen-deprivation conditions, a dependence that has been observed in the clinic for other antiandrogens such as flutamide (15). Interestingly, although the switch did not drive proliferation of F876L-bearing clones *in vitro* (Supplementary Fig. S14), we observed a marked dependence on MDV3100 for growth *in vivo* when the F876L-bearing cells were implanted into castrated male mice (Fig. 5E). Although control (C1) tumors showed immediate stasis upon MDV3100 treatment, resistant tumors (clone #1) failed to grow until stimulated by MDV3100 (Fig. 5E). Specifically, after a prolonged period of stasis, 10 of 15 mice treated with MDV3100 developed rapidly growing tumors compared with two of 15 in the vehicle group

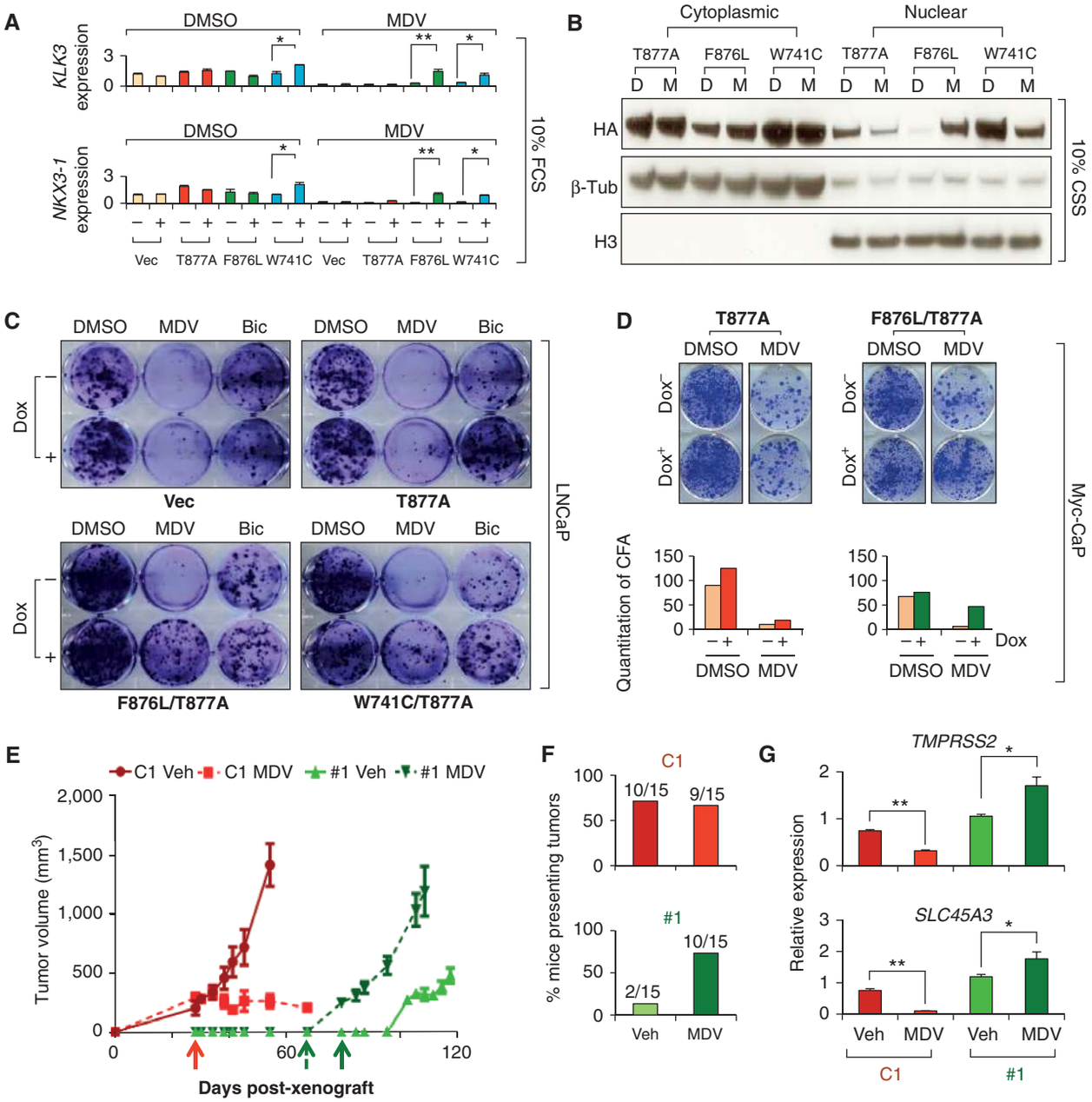

Figure 5. Prostate cancer cells engineered to overexpress AR$^{F876L/T877A}$ are genetically and phenotypically resistant to MDV3100. **A,** qPCR analysis of *KLK3* (top) and *NKX3-1* (bottom) expression in various engineered lines [vector controls (Vec); T877A; F876L/T877A, F876L; W741C/T877A, W741C]. All lines were pretreated with vehicle (−) or doxycycline (+) for 3 days before treatment with DMSO (left) or 10 μmol/L MDV3100 (right) for 24 hours in 10% FCS. *TBP* was used to normalize expression. Data represent mean ± SEM; $n = 3$. *, $P < 0.05$; **, $P < 0.01$ (Student *t* test). **B,** Western blot analysis of exogenous AR (HA) expression in cytoplasmic and nuclear fractions isolated from various engineered lines treated with DMSO (D) or 10 μmol/L MDV3100 (M) in media supplemented with 10% CSS. All lines were pretreated with Dox for 3 days before treatment with DMSO or MDV3100 for 24 hours. F876L, F876L/T877A; W741C, W741C/T877A. β-Tubulin (β-Tub) and histone H3 (H3) were probed to validate purity of cytoplasmic and nuclear fractions respectively. **C,** colony formation assays of various engineered lines (Dox$^{-/+}$) treated with DMSO, 1 μmol/L MDV3100 (MDV), or 1 μmol/L bicalutamide (Bic) for 3 to 4 weeks. Representative experiment from three independent experiments is shown. **D,** top, colony formation assays of Myc-CaP cells engineered to express AR^{T877A} (left) or AR$^{F876L/T877A}$ (right; Dox$^{-/+}$) treated with DMSO (left wells) or 10 μmol/L MDV3100 (right wells; MDV) for approximately 14 days. Bottom, quantitation of colony formation data by ImageJ. **E,** tumor volume measurements of control (C1; red) and resistant clone #1 (#1; green), tumors treated with vehicle (Veh) or 30 mg/kg MDV3100 (MDV). Solid red and green arrows indicate the day daily administration of MDV3100 was initiated in control (C1) and clone #1 (#1) mice, respectively. Dashed green arrow highlights 2 consecutive days of treatment with MDV3100 before a drug holiday in 15 of 30 mice injected with clone #1 (#1; dark green). $n = 7$ to 8 tumors for all groups except #1 vehicle ($n = 2$). Data represent mean ± SEM. **F,** bar graphs showing percentage of mice growing palpable tumors (numbers above bars represent number of mice presenting tumors). **G,** qPCR analysis of *TMPRSS2* and *SLC45A3* expression in control (C1) and resistant (#1) tumors treated with vehicle or MDV3100 (MDV). *TBP* was used to normalize expression. Data represent mean ± SEM; $n = 3$ for all groups except C1 vehicle treated, $n = 2$. *, $P < 0.05$; **, $P < 0.01$ (Student *t* test).

(P = 0.0078; Fisher exact t test, two-tailed), whereas the tumor take rates of control cells (C1) were indistinguishable (9 of 15 vs. 10 of 15; Fig. 5F). Furthermore, resistant tumors continued to grow in the presence of MDV3100, in agreement with earlier *in vitro* observations (Fig. 1C), cumulatively suggesting that AR^{F876L}–bearing cells require MDV3100 for growth *in vivo*. No significant body weight loss was observed during the treatment period in all four groups (Supplementary Fig. S15A and S15B). Endpoint molecular analysis confirmed an agonist switch of MDV3100 associated with the F876L mutation *in vivo* as resistant tumors treated with MDV3100 showed modestly higher AR pathway activity, as shown by AR target gene expression, relative to vehicle-treated resistant tumors, and significantly higher activity relative to vehicle-treated control tumors (Fig. 5G). These data cumulatively highlight the dependence of F876L-bearing cells to MDV3100 for *in vivo* growth under androgen-deprivation conditions.

Targeting CDK4/6 as a Therapeutic Strategy for Overcoming MDV3100 Resistance

Having established that AR^{F876L} can promote resistance to MDV3100 under various genetic contexts *in vitro* and *in vivo*, we next aimed to develop rational strategies to antagonize the mutant allele. As an alternative to developing novel antiandrogens that continue to target the hypermutable ligand-binding pocket of AR (16), we aimed to identify therapeutic strategies that may be more sustainable in the clinic. To this end, we observed a significant enrichment for genes belonging to "cell cycle" and "E2F1 activation" gene sets in addition to "AR activation" in strongly resistant clones treated with MDV3100 (Fig. 2A), suggesting that these clones may potentially maintain proliferation under MDV3100-treatment conditions through continued expression of E2F1 target genes. This is an appealing hypothesis as androgen signaling, a critical regulator of G_1–S transition, is known to promote active CDK4/cyclin D1 assembly and hence activation of E2F1 function (17). Consistent with this notion, we observed that MDV3100 treatment suppressed expression of the E2F1 target genes *DHFR* and *TK1* in a control line, confirming AR signaling as a regulator of E2F1 function. In contrast, F876L-bearing cells were capable of maintaining higher expression of *DHFR* and *TK1* under MDV3100-treatment conditions relative to a control line (Fig. 6A). On the basis of these data, we reasoned that E2F1 activity may serve as a downstream effector of AR signaling, and as such, regulators of E2F1 function may serve as critical therapeutic nodes when AR-directed therapies become ineffective. In agreement with this hypothesis, we found that growth of strongly resistant clones (Fig. 6B) and LNCaP lines engineered to express $AR^{F876L/T877A}$ (Fig. 6C) were as sensitive to CDK4/6 inhibitors LEE011 (18) and PD033299 as bicalutamide. Interestingly, response to CDK4/6 inhibition was not only limited to F876L-bearing cells, as androgen-independent 22Rv1 cells—a prostate cancer line expressing WT AR and capable of maintaining AR signaling and expression of *DHFR* and *TK1* under MDV3100 treatment conditions (Fig. 6D)—also showed strong sensitivity to CDK4/6 inhibition (Fig. 6E). These data cumulatively suggest that targeting CDK4/6 function may serve as an effective strategy for treatment of multiple mechanisms of resistance to MDV3100 and likely androgen independence in general.

DISCUSSION

In this study, we functionally confirmed an agonist switch mutation (F876L) in AR that drives phenotypic resistance to MDV3100. Furthermore, we highlighted the therapeutic potential of targeting downstream effectors of AR signaling, such as CDK4/6, when AR-directed therapies become ineffective. Collectively, these data imply (i) that patients bearing a preexisting *AR*-F876L mutation might show clinical progression of the disease in response to MDV3100 treatment, (ii) that patients developing the F876L mutation upon MDV3100 treatment might benefit from drug withdrawal, and (iii) that all F876L-bearing patients (preexisting or acquired) might respond favorably to existing antiandrogens and CDK4/6 inhibitors (Fig. 7). Therefore, screening patients to identify this mutation will aid in predicting drug sensitivity and guide alternate clinical management strategies.

F876L: Hotspot Mutation in *AR* in Response to MDV3100 Treatment

The relatively quick emergence of the F876L mutation during *in vitro* selection (Fig. 3A and B) initially suggested that this mutation was likely preexisting at a low frequency. However, the fact that two independent nucleotide substitutions led to the F876L mutation during *in vivo* selection (Fig. 3D and E) implies that the mutation may have been acquired during treatment. Because LNCaP cells possess defects in the mismatch repair (MMR) mechanism, deficiencies found to also exist in a subset of prostate cancer (19), it is conceivable that they may more easily acquire this mutation (either with or without MDV3100 treatment). However, the fact that Balbas and colleagues (16) also reported the spontaneous emergence of F876L upon prolonged treatment of CWR22PC cells, a line that is believed to possess an intact MMR mechanism, suggests that F876L may truly be a hotspot mutation that may possess the capacity to confer resistance in prostate tumors irrespective of the MMR status.

Agonist Switch Suggests a Treatment Withdrawal Effect for MDV3100

In some patients that become refractory to antiandrogen therapy, discontinuation of treatment often leads to clinical improvement. This "antiandrogen withdrawal syndrome" has been reported for flutamide (20), bicalutamide (21), and other nonsteroidal and steroidal antiandrogens (22–24). In a subset of patients presenting "addiction" to antiandrogen therapy, mutations in *AR* that promote an agonist switch have been identified and considered to be one potential mechanism driving growth during treatment (15). In the current study, we also observed an "addiction" phenomenon as the growth of an F876L-bearing cell line (clone #1) became dependent on MDV3100 for growth *in vivo* (Fig. 5E). These parallels imply that refractory patients bearing the AR^{F876L} variant may, at least temporarily, benefit from withdrawal of MDV3100 in the clinic.

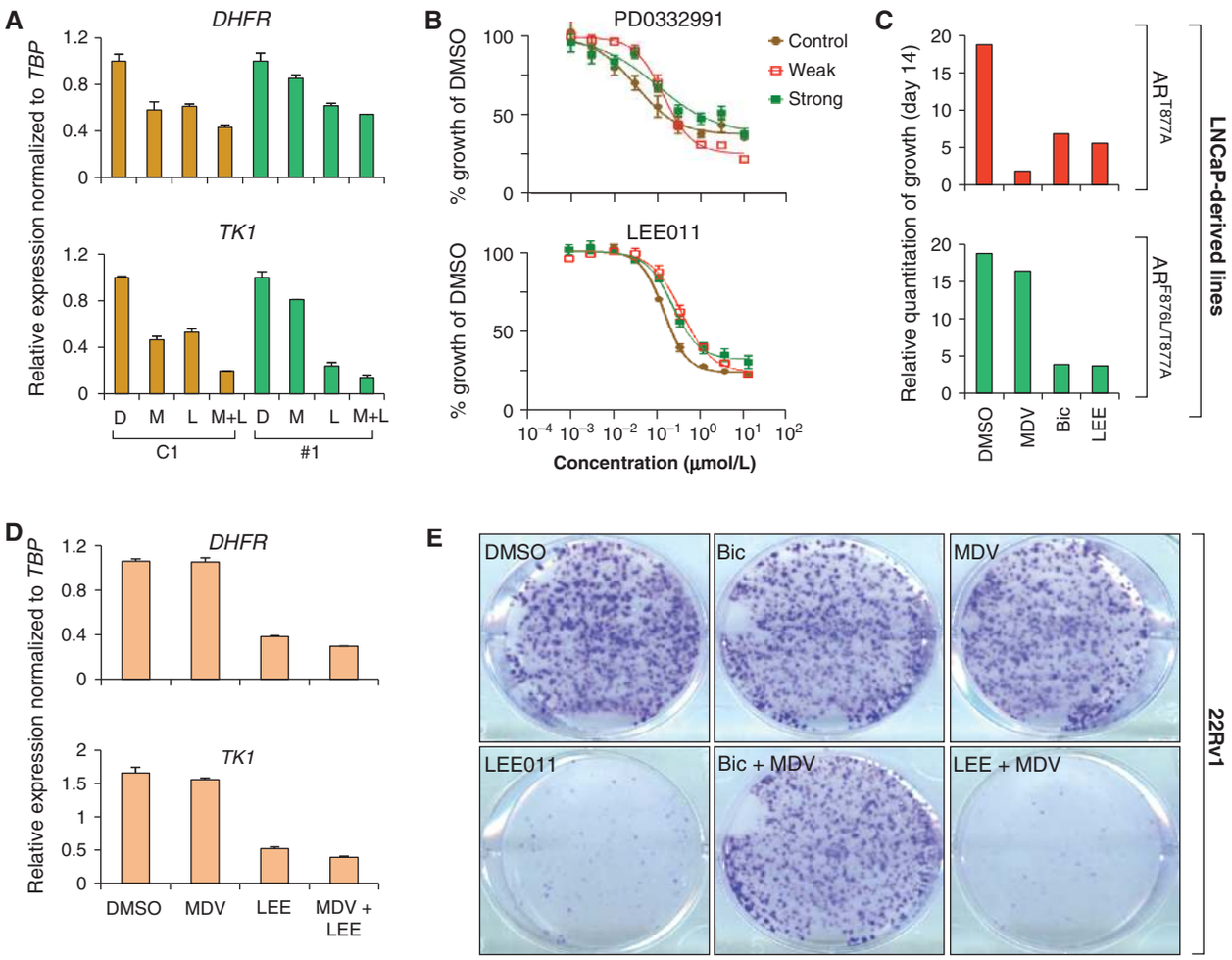

Figure 6. Targeting CDK4/6 reduces proliferation of MDV3100-resistant prostate cancer cell lines. **A,** qPCR analysis of E2F1 targets *DHFR* and *TK1* in C1 and clone #1 lines upon treatment with DMSO (D), 10 μmol/L MDV3100 (M), 10 μmol/L LEE011 (L), or 10 μmol/L MDV3100 and 10 μmol/L LEE011 (M+L) for 24 hours. **B,** average growth inhibition curves for the three controls (brown line) and seven resistant clones (green and red) treated with PD033299 (top) and LEE011 (bottom). Data presented as percentage of growth relative to DMSO treatment condition as measured by CellTiter-Glo assay. **C,** relative quantitation of data from colony formation assays of AR^{T877A} and $AR^{F876L/T877A}$ lines treated with DMSO, 10 μmol/L MDV3100 (MDV), 10 μmol/L bicalutamide (Bic), or 10 μmol/L LEE011 (LEE) for 28 days (quantitated by ImageJ). **D,** qPCR analysis of E2F1 targets *DHFR* and *TK1* in the androgen-independent 22Rv1 line treated with DMSO, 10 μmol/L MDV3100 (MDV), 10 μmol/L LEE011 (LEE), or 10 μmol/L MDV3100 and 10 μmol/L LEE011 (MDV+LEE) for 48 hours. **E,** colony formation assays of 22Rv1 cells treated with various indicated compounds (DMSO, Bic, MDV, or LEE) for 14 days.

Alternative Therapeutic Strategies

The frequent emergence of an agonist switch as a resistance mechanism to antiandrogens necessitates that (i) more potent compounds with better therapeutic indices be developed, (ii) alternate methods to target AR be sought, or (iii) non-AR–targeting therapeutic strategies be explored. To address the first point, Clegg and colleagues (4) recently developed ARN-509, an antiandrogen that is more potent, has a higher therapeutic index, and has a longer half-life than MDV3100, all of which might translate to less-frequent resistance. Interestingly, two independent groups recently reported the spontaneous emergence of the F876L mutation in *AR* as an agonist switch specific for both MDV3100 and ARN-509 (16, 25). To overcome this mutation, Balbas and colleagues (16) coupled modeling with focused chemical screens to discover novel antiandrogens that effectively antagonized AR-WT and AR-F876L. Although too early to predict, if agonist switch conferring mutations develop to these novel compounds, then applying strategies that may be less amenable to resistance by mutations in the AR ligand-binding pocket should be explored. Strategies such as combining two antiandrogens (in combination or sequentially), blocking activation function 1 (AF1; ref. 26) or AF2 (26, 27) functions of AR, or development of compounds that destabilize/degrade AR or hinder AR nuclear translocation might be also considered. Finally, non-AR–targeting therapies may also serve as a viable strategy. To this end, we found that inhibiting CDK4/6 potently targeted both strongly resistant clones (Fig. 6B) and LNCaPs engineered to overexpress $AR^{F876L/T877A}$ (Fig. 6C), implying that targeting downstream effectors of AR signaling may serve as a viable strategy for overcoming this mutation-based resistance mechanism. Even more generally, inhibition of CDK4/6

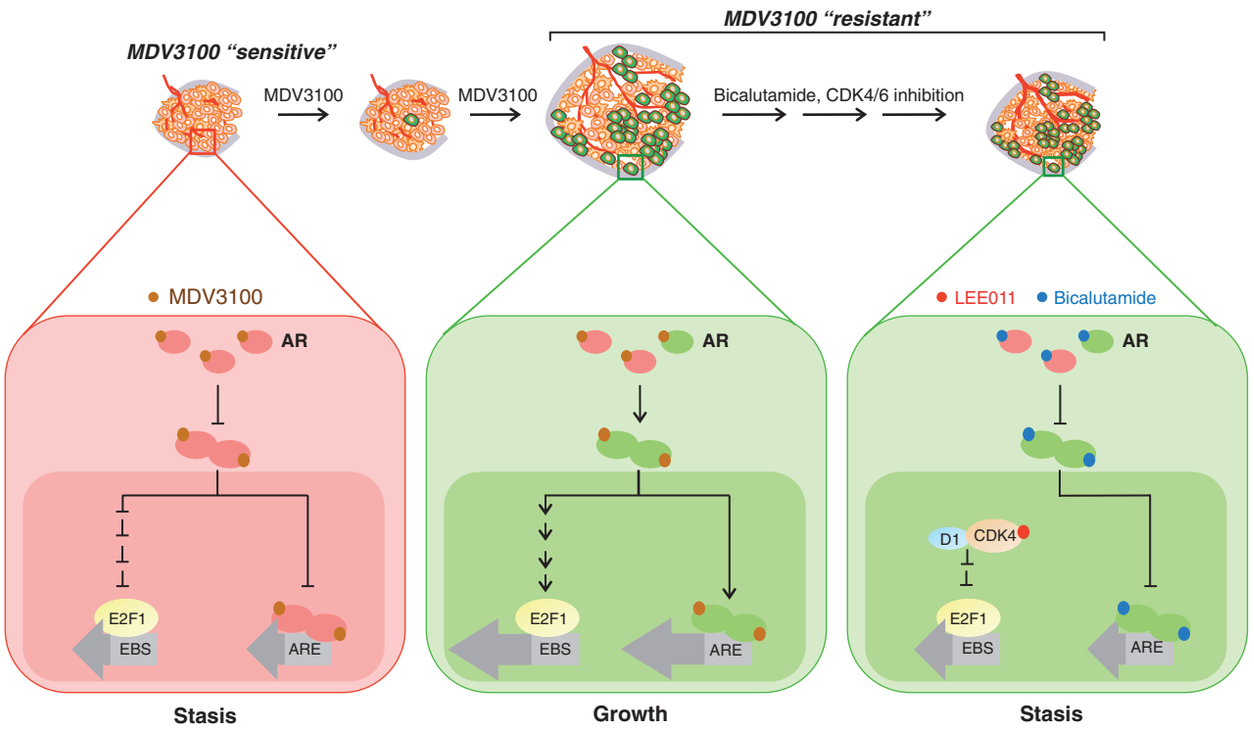

Figure 7. Schematic representation of the therapeutic strategies that can be applied to target AR^{F876L}. Left, MDV3100 (brown circles) suppresses expression of E2F1 and canonical AR target genes upon binding to AR-WT (red ovals). Middle, AR^{F876L} (green ovals) uses MDV3100 as an agonist and thus maintains expression of E2F1 and canonical AR target genes. Right, targeting CDK4/6 or AR with structurally distinct antiandrogens can hinder proliferation through suppression of E2F1 and canonical AR target genes, respectively. Length of gray arrow represents relative level of pathway activity. Red and blue circles represent CDK4/6 inhibitor and bicalutamide, respectively. EBS, E2F1-binding sites; ARE, androgen-responsive elements.

also targeted weakly resistant LNCaP clones (Fig. 6B) and MDV3100-resistant 22Rv1 cells (Fig. 6E)—prostate cancer lines lacking AR^{F876L}—implying that this therapy may be applied to overcome multiple mechanisms of resistance to MDV3100 and androgen-independence in general. In support of our findings, several reports have suggested that retinoblastoma (RB) loss plays a critical role in prostate cancer development and resistance to AR-directed therapies (28). More relevantly, consistent with our findings, a recent study has reported the use of CDK4/6 inhibitors as an effective therapeutic to target early- and late-stage prostate cancer that is mechanistically dependent on RB (29). Because a significant fraction of CRPCs maintain functional RB, we speculate that inhibition of CDK4/6 may serve as a viable approach for treating resistance to AR-directed therapies in a large subset of patients.

METHODS

Cell Culture

LNCaP-FGC and PC3 cells were maintained in RPMI-1640 media with 10% FCS (Hyclone) or 10% CSS (Omega; cat# fb-04) as indicated. 22Rv1 cells were maintained in RPMI-1640 media with 10% FCS. VCaP cells were maintained in Dulbecco's Modified Eagle Medium (DMEM) with 10% FCS or 10% CSS. Myc-CaP cells were maintained in DMEM with 10% FCS. 293FT cells were maintained in DMEM supplemented with 10% FCS and 1 × Non-Essential Amino Acids (NEAA). All lines, except Myc-CaP cells, were obtained from the American Type Culture Collection and cells were tested and authenticated by single-nucleotide polymorphism fingerprinting. Myc-CaP cells were kindly provided by Dr. Charles Sawyers (Human Oncology and Pathogenesis Program, Memorial Sloan-Kettering Cancer Center, New York, NY) and were not further tested or authenticated.

Generation of Spontaneous MDV3100-Resistant LNCaP Clones In Vitro

Two million LNCaP cells were seeded into four 150-cm^2 tissue culture dishes in phenol red–free RPMI-1640 media supplemented with 10% FCS. The next day, DMSO and ethanol (control 1, C1), DMSO and 1.0 nmol/L R1881 (control 2, C2), 1 μmol/L MDV + 1.0 nmol/L R1881 (control 3, C3), and 1 μmol/L MDV3100 were added to dishes 1 to 4, respectively. Cells were reseeded into 150-cm^2 dishes supplemented with the appropriate treatments once each week. Media and compound were replaced for dish 4 once every week. Once resistant clones emerged, media was aspirated from dish 4. Trypsin-soaked 3-mm sterile cloning discs (Scienceware; cat# 17-2.X) were used to overlay the resistant clones and following a 1- to 2-minute incubation, cloning discs were transferred to 24-well plates with phenol red–free RPMI-1640 media supplemented with 10% FCS and MDV3100. Cells from control dishes 1 to 3 were maintained until resistant clones were cryopreserved to maintain a constant culture time for control and experimental lines.

Generation of Stable Transduced Lines

Codon-optimized cDNAs encoding WT or mutant ARs were synthesized (DNA2.0) and subcloned into the pLKO-TREX-HA-Neo (Invitrogen). Lentiviruses were produced by transfecting 293FT cells with VSVG:deltaR8.9:cDNA constructs at a ratio of 1:2.5:1.25. Virus

was harvested 2 to 3 days after transfection, filtered, and used to infect LNCaP, MyC-CaP, and VCaP cell cultures in the presence of 8 μg/mL polybrene. Infected cells were maintained in neomycin for 3 weeks. In all cases, at least 1,000 independent clones were pooled to generate stable cell lines to avoid clonal variations. Stable cell lines infected with control vectors were generated in parallel for use as experimental controls.

Microarray

A total of 3×10^5 cells were seeded in 6-well plates 2 to 3 days before treatment with DMSO or 10 μmol/L MDV3100 for 24 hours. Total RNA was isolated from cells using the Qiagen RNeasy Kit. RNA integrity and purity were assessed with the RNA 6000 Nano LabChip system on a Bioanalyzer 2100 (Agilent Technologies). Generation of labeled cDNA and hybridization to Affymetrix GeneChip Human Genome U133 Plus 2.0 Array (Affymetrix Inc.) was conducted using standard protocols as previously described (8).

Expression Analysis

Probe sets from the Affymetrix gene expression datasets were normalized using MAS5 with a trimmed-mean target of 150 and $\log_2$-transformed. Probe sets were then filtered for inclusion only if their maximum value over different samples was at least 5. Ordinary least squares was conducted using 0 to 1 indicator variables as the covariates; one indicator was used to represent the baseline (untreated sample) of each clone, and three indicator variables represented treatment with MDV3100 for each of the classes of samples (control, weakly resistant clones, and strongly resistant clones). This regression was used to generate nominal *P* values and regression coefficients (i.e., fold changes). Individual probe sets were considered significantly differentially expressed if their fold change was 1.5 or more, with a nominal $P \leq 0.05$.

Gene Set Enrichment Analysis

GSEA was performed by calculating the AR gene signature (30) enrichment in the top-ranked genes following treatment of control, weakly and strongly resistant clones with MDV3100. Blue line represents expressed probe set position and is ranked by average fold change; only those probe sets expressed at a MAS5-150 level of at least 32 in at least one sample are included. The red lines indicate where the probe sets mapping to genes in the AR gene signatures appear in our dataset, gray lines indicate probe sets that do not pass nominal significance, and the taller red line represents probe sets with a fold change of at least 1.5 and a nominal P value less than 0.05. The black curve shows the cumulative sum of the probe sets in the AR gene signature, and the dotted line represents the hypothetical cumulative sum for a random list of genes, which are unenriched.

Pathway Enrichment Scores

For the candidate signature (30), a two-tailed Fisher exact test was used to determine whether probe sets representing genes in those signatures were under- or over represented in the set of probe sets that were up- or downregulated at least 1.5-fold compared with expressed but nondifferentially expressed probe sets, with a nominal *P* value of 0.05 or less. For an unbiased approach, pathways derived from Gene Ontology (GO) terms and transcription factor networks were analyzed for overrepresentation via a one-tailed interpolated Fisher exact test, using genes that varied 1.5-fold or more with a nominal *P* value of 0.05 or less compared with all genes represented on the array; Benjamini–Hochberg correction was then applied to these *P* values (8).

Sanger Sequencing

Genomic DNA was isolated from various 1 μmol/L MDV3100-resistant clones and appropriate control lines using the Blood and Tissue DNAeasy Kit (Qiagen; cat# 69581) according to the manufacturer's directions. Primers were used to amplify *AR* exon 8 (the site of the F876L mutation; forward: 5′-ATTGCGAGAGAGCTGCATCA-3′; reverse: 5′-TTCTCGTCACTATTGGCCTC-3′) and the amplified cDNA was sequenced by Genewiz using the same primers. Trace files were analyzed to confirm the presence of the F876L mutation.

Quantitative Real-Time PCR

For spontaneous clones, 2×10^5 cells were seeded in 6-well plates in RPMI-1640 supplemented with 10% FCS for 2 days before treatment with various compounds for 24 hours. Alternatively, for experiments involving androgen depletion, 2×10^5 cells were seeded and grown in 6-well plates in phenol red–free RPMI-1640 supplemented with 10% FCS for 2 days. Media was aspirated and replaced with phenol red–free RPMI-1640 supplemented with 10% CSS for 3 to 4 days before treatment with various compounds for 24 hours. Similar protocols were applied for genetically engineered lines except that cells were pretreated with doxycycline (Dox) for at least 2 days before treatment with various compounds to allow sufficient transgene expression. Total RNA was extracted using the RNeasy Plus Mini Kit (Qiagen; cat# 74136) according to the manufacturer's instructions. One to 2 μg of total RNA was used for cDNA synthesis using a high-capacity cDNA reverse transcription kit (Applied Biosystems; cat# 4368813). cDNA from each sample was diluted 15- to 20-fold and real-time PCR was conducted in triplicate using gene-specific primers and FastStart Universal Probe Master Mix (Rox; Roche Applied Science) on an ABI 7900HT series PCR machine. Expression levels were normalized to *TBP* expression. All analysis was conducted using the SDS2.3 software. The following gene-specific primers (Invitrogen) were used: *AR* (Hs00171172_m1), *KLK3* (Hs02576345_m1), *NKX3-1* (Hs00171834_m1), *TMPRSS2* (Hs01120965_m1), *SLC45A3* (Hs00263832_m1), *TBP* (Hs00427620_m1), *DHFR* (Hs00758822_s1), and *TK1* (Hs01062125_m1).

In Vivo *Tumorigenesis* Assays

Ten million LNCaP cells (C1, clone #1) mixed 1:1 with Matrigel were injected subcutaneously into the flanks of castrated 7- to 8-week-old male nu/nu mice. Tumor-bearing mice (tumor volume = 150–300 mm^3) were treated with vehicle or 30 mg/kg MDV3100 daily. Tumors were measured using calipers, and tumor volumes were calculated using length × $width^2/2$. Data are expressed as mean ± SEM. All animal experiments were carried out in compliance with the guidelines of the Novartis Biomedical Research Animal Care and Use Committee protocols and regulations.

Statistical Analysis

Results were reported as the mean ± SEM. A two-sided independent Student *t* test without equal variance assumption was conducted to analyze gene expression levels and endpoints of *in vitro* luciferase assays. For gene set enrichment analysis, *P* values shown are based on a two-tailed Fisher exact test comparing probe sets in the gene signature that pass significance to those that do not, versus the significance/insignificance of all other probe sets. For animal experiments, a two-tailed Fisher exact test was conducted to determine the significance in percentage of mice growing palpable tumors in each group.

Accession Number

Gene expression microarray data used to analyze differential gene expression upon treatment with MDV3100 versus DMSO in spontaneous and engineered lines has been deposited at the National Center for Biotechnology Information (NCBI) Gene Expression Omnibus with the accession numbers GSE44924 and GSE44927, respectively.

Additional experimental procedures are listed in the Supplementary Methods.

Disclosure of Potential Conflicts of Interest

M. Korpal has ownership interest (including patents) in Novartis Institutes for BioMedical Research. V.G. Cooke has ownership interest (including patents) in Novartis Institutes for BioMedical Research. T.M. Roberts has received a commercial research grant from Novartis and is a consultant/advisory board member of the same. W.R. Sellers is employed as VP/Global Head of Oncology at Novartis and has ownership interest (including patents) in the same. P. Zhu has ownership interest (including patents) in Novartis. No potential conflicts of interest were disclosed by the other authors.

Authors' Contributions

Conception and design: M. Korpal, S. Kim, W.R. Sellers, P. Zhu
Development of methodology: M. Korpal, X. Gao, D.A. Ruddy, P. Zhu
Acquisition of data (provided animals, acquired and managed patients, provided facilities, etc.): M. Korpal, X. Gao, D.P. Rakiec, J. Yuan, S.G. Kovats, V.G. Cooke, J.E. Monahan
Analysis and interpretation of data (e.g., statistical analysis, biostatistics, computational analysis): M. Korpal, J.M. Korn, X. Gao, D.A. Ruddy, S. Doshi, S. Kim, W.R. Sellers
Writing, review, and/or revision of the manuscript: M. Korpal, X. Gao, S. Kim, F. Stegmeier, T.M. Roberts, W.R. Sellers, W. Zhou, P. Zhu
Administrative, technical, or material support (i.e., reporting or organizing data, constructing databases): M. Korpal, D.A. Ruddy, W.R. Sellers
Study supervision: M. Korpal, T.M. Roberts, W. Zhou, P. Zhu

Acknowledgments

The authors thank Dmitriy Sonkin for assistance with generation of AR pathway activity scores, Ming-hong Hao and Greg Paris for help with computational modeling, Travis Stams and Christina Kirby for crystal structure analysis, and Heather A. Keane for ordering of key reagents. The authors also thank Nicholas Keen, Michael Schlabach, Dale Porter, Raymond Pagliarini, and Mario A. Blanco for critical reading of the article and helpful suggestions.

Grant Support

All studies were funded by Novartis Institutes for BioMedical Research. M. Korpal is a recipient of the presidential postdoctoral fellowship from Novartis Institutes for BioMedical Research.

Received April 1, 2013; revised July 9, 2013; accepted July 9, 2013; published OnlineFirst July 10, 2013.

REFERENCES

1. Kawata H, Ishikura N, Watanabe M, Nishimoto A, Tsunenari T, Aoki Y. Prolonged treatment with bicalutamide induces androgen receptor overexpression and androgen hypersensitivity. Prostate 2010;70:745–54.
2. Jemal A, Siegel R, Ward E, Hao Y, Xu J, Murray T, et al. Cancer statistics, 2008. CA Cancer J Clin 2008;58:71–96.
3. Scher HI, Sawyers CL. Biology of progressive, castration-resistant prostate cancer: directed therapies targeting the androgen-receptor signaling axis. J Clin Oncol 2005;23:8253–61.
4. Clegg NJ, Wongvipat J, Joseph JD, Tran C, Ouk S, Dilhas A, et al. ARN-509: a novel antiandrogen for prostate cancer treatment. Cancer Res 2012;72:1494–503.
5. Jemal A, Siegel R, Xu J, Ward E. Cancer statistics, 2010. CA Cancer J Clin 2010;60:277–300.
6. Chen CD, Welsbie DS, Tran C, Baek SH, Chen R, Vessella R, et al. Molecular determinants of resistance to antiandrogen therapy. Nat Med 2004;10:33–9.
7. Kim W, Ryan CJ. Androgen receptor directed therapies in castration-resistant metastatic prostate cancer. Curr Treat Options Oncol 2012;13:189–200.
8. Wiederschain D, Chen L, Johnson B, Bettano K, Jackson D, Taraszka J, et al. Contribution of polycomb homologues Bmi-1 and Mel-18 to medulloblastoma pathogenesis. Mol Cell Biol 2007;27:4968–79.
9. Tran C, Ouk S, Clegg NJ, Chen Y, Watson PA, Arora V, et al. Development of a second-generation antiandrogen for treatment of advanced prostate cancer. Science 2009;324:787–90.
10. Tan J, Sharief Y, Hamil KG, Gregory CW, Zang DY, Sar M, et al. Dehydroepiandrosterone activates mutant androgen receptors expressed in the androgen-dependent human prostate cancer xenograft CWR22 and LNCaP cells. Mol Endocrinol 1997;11:450–9.
11. Fenton MA, Shuster TD, Fertig AM, Taplin ME, Kolvenbag G, Bubley GJ, et al. Functional characterization of mutant androgen receptors from androgen-independent prostate cancer. Clin Cancer Res 1997;3:1383–8.
12. Veldscholte J, Ris-Stalpers C, Kuiper GG, Jenster G, Berrevoets C, Claassen E, et al. A mutation in the ligand binding domain of the androgen receptor of human LNCaP cells affects steroid binding characteristics and response to anti-androgens. Biochem Biophys Res Commun 1990;173:534–40.
13. Hara T, Miyazaki J, Araki H, Yamaoka M, Kanzaki N, Kusaka M, et al. Novel mutations of androgen receptor: a possible mechanism of bicalutamide withdrawal syndrome. Cancer Res 2003;63:149–53.
14. Zhu P, Baek SH, Bourk EM, Ohgi KA, Garcia-Bassets I, Sanjo H, et al. Macrophage/cancer cell interactions mediate hormone resistance by a nuclear receptor derepression pathway. Cell 2006;124:615–29.
15. Suzuki H, Akakura K, Komiya A, Aida S, Akimoto S, Shimazaki J. Codon 877 mutation in the androgen receptor gene in advanced prostate cancer: relation to antiandrogen withdrawal syndrome. Prostate 1996;29:153–8.
16. Balbas MD, Evans MJ, Hosfield DJ, Wongvipat J, Arora VK, Watson PA, et al. Overcoming mutation-based resistance to antiandrogens with rational drug design. eLife 2013;2:e00499.
17. Schiewer MJ, Den R, Hoang DT, Augello MA, Lawrence YR, Dicker AP, et al. mTOR is a selective effector of the radiation therapy response in androgen receptor-positive prostate cancer. Endocr Relat Cancer 2012;19:1–12.
18. Rader JA, Hart L, Russell M, Nakazawa M, Belcastro L, Martinez D, et al. CDK4/CDK6 inhibition is potently active in a definable subset of human neuroblastomas [abstract]. In: Proceedings of the Annual Meeting of the American Association for Cancer Research; 2013 Apr 6–10; Washington, DC. Philadelphia (PA): AACR; 2013. Abstract nr 2744.
19. Chen Y, Wang J, Fraig MM, Metcalf J, Turner WR, Bissada NK, et al. Defects of DNA mismatch repair in human prostate cancer. Cancer Res 2001;61:4112–21.
20. Kelly WK, Scher HI. Prostate specific antigen decline after antiandrogen withdrawal: the flutamide withdrawal syndrome. J Urol 1993;149:607–9.
21. Small EJ, Carroll PR. Prostate-specific antigen decline after casodex withdrawal: evidence for an antiandrogen withdrawal syndrome. Urology 1994;43:408–10.
22. Miyamoto H, Rahman MM, Chang C. Molecular basis for the antiandrogen withdrawal syndrome. J Cell Biochem 2004;91:3–12.
23. Huan SD, Gerridzen RG, Yau JC, Stewart DJ. Antiandrogen withdrawal syndrome with nilutamide. Urology 1997;49:632–4.
24. Sella A, Flex D, Sulkes A, Baniel J. Antiandrogen withdrawal syndrome with cyproterone acetate. Urology 1998;52:1091–3.
25. Joseph JD, Lu N, Qian J, Sensintaffar J, Shao G, Brigham D, et al. A clinically relevant androgen receptor mutation confers resistance to

2nd generation anti-androgens enzalutamide and ARN-509. Cancer Discov 2013 Jun 18. [Epub ahead of print].
26. Gao W. Peptide antagonist of the androgen receptor. Curr Pharm Des 2010;16:1106–13.
27. Andersen RJ, Mawji NR, Wang J, Wang G, Haile S, Myung JK, et al. Regression of castrate-recurrent prostate cancer by a small-molecule inhibitor of the amino-terminus domain of the androgen receptor. Cancer Cell 2010;17:535–46.
28. Balk SP, Knudsen KE. AR, the cell cycle, and prostate cancer. Nucl Recept Signal 2008;6:e001.
29. Comstock CE, Augello MA, Goodwin JF, de Leeuw R, Schiewer MJ, Ostrander WF, et al. Targeting cell cycle and hormone receptor pathways in cancer. Oncogene 2013 May 27. [Epub ahead of print].
30. Mendiratta P, Mostaghel E, Guinney J, Tewari AK, Porrello A, Barry WT, et al. Genomic strategy for targeting therapy in castration-resistant prostate cancer. J Clin Oncol 2009;27:2022–9.